Received: 9 December 2020 | Revised: 14 April 2021 | Accepted: 19 April 2021

DOI: 10.1111/apha.13668

REGULAR PAPER

ACTA PHYSIOLOGICA

Pharmacological HIF-PHD inhibition reduces renovascular resistance and increases glomerular filtration by stimulating nitric oxide generation

Mikhail Burmakin[1] | **Angelica Fasching**[1] | **Hanako Kobayashi**[2] | **Andrés A. Urrutia**[3] | **Anastasios Damdimopoulos**[4] | **Fredrik Palm**[1] | **Volker H. Haase**[1,2,5]

[1]Section of Integrative Physiology, Department of Medical Cell Biology, Uppsala University, Uppsala, Sweden

[2]Department of Medicine, Vanderbilt University Medical Center and Vanderbilt University School of Medicine, Nashville, TN, USA

[3]Unidad de Investigación Hospital de Santa Cristina, Instituto de Investigación del Hospital Universitario La Princesa, Universidad Autónoma de Madrid, Madrid, Spain

[4]Bioinformatics and Expression Analysis Core Facility, Department of Biosciences and Nutrition, Karolinska Institute, Stockholm, Sweden

[5]Department of Molecular Physiology and Biophysics, Vanderbilt University School of Medicine, Nashville, TN, USA

Correspondence
Volker H. Haase, Division of Nephrology & Hypertension, Department of Medicine, Vanderbilt University Medical Center, C-3119A MCN, 1161 21st Avenue So., Nashville, TN 37232-2372, USA.
Email: volkerhhaase@gmail.com

Funding information
VINNOVA; Uppsala Universitet; Vetenskapsrådet

Abstract

Aim: Hypoxia-inducible factors (HIFs) are O_2-sensitive transcription factors that regulate multiple biological processes which are essential for cellular adaptation to hypoxia. Small molecule inhibitors of HIF-prolyl hydroxylase domain (PHD) dioxygenases (HIF-PHIs) activate HIF-dependent transcriptional programs and have broad clinical potential. HIF-PHIs are currently in global late-stage clinical development for the treatment of anaemia associated with chronic kidney disease. Although the effects of hypoxia on renal haemodynamics and function have been studied in animal models and in humans living at high altitude, the effects of pharmacological HIF activation on renal haemodynamics, O_2 metabolism and metabolic efficiency are not well understood.

Methods: Using a cross-sectional study design, we investigated renal haemodynamics, O_2 metabolism, gene expression and NO production in healthy rats treated with different doses of HIF-PHIs roxadustat or molidustat compared to vehicle control.

Results: Systemic administration of roxadustat or molidustat resulted in a dose-dependent reduction in renovascular resistance (RVR). This was associated with increased glomerular filtration rate (GFR), urine flow and tubular sodium transport rate (T_{Na}). Although both total O_2 delivery and T_{Na} were increased, more O_2 was extracted per transported sodium in rats treated with high-doses of HIF-PHIs, suggesting a reduction in metabolic efficiency. Changes in RVR and GFR were associated with increased nitric oxide (NO) generation and substantially suppressed by pharmacological inhibition of NO synthesis.

Conclusions: Our data provide mechanistic insights into dose-dependent effects of short-term pharmacological HIF activation on renal haemodynamics, glomerular filtration and O_2 metabolism and identify NO as a major mediator of these effects.

KEYWORDS

glomerular filtration rate, hypoxia-inducible factor, molidustat, nitric oxide, prolyl hydroxylase domain, roxadustat

1 | INTRODUCTION

Small molecule inhibitors of hypoxia-inducible factor (HIF)-prolyl hydroxylase domain (PHD) O_2 sensors (HIF-PHIs) are a promising new class of orally administered drugs that mimic hypoxia responses and have broad therapeutic potential.[1,2] The HIF/PHD O_2-sensing pathway regulates multiple cellular responses to hypoxia and is involved in numerous disease states including ischemia-reperfusion injury, pulmonary arterial hypertension, cancer and abnormal erythropoiesis.[3] In the context of anaemia therapy, HIF-PHIs promote erythropoiesis through an increase in HIF activity, which stimulates the production of endogenous erythropoietin (EPO) in kidney and liver and promotes iron uptake and mobilization.[1] However, given the breadth of HIF-regulated biological processes, HIF-PHI therapy is expected to have clinical effects beyond erythropoiesis that may be beneficial for patients with chronic kidney disease (CKD) or could potentially cause harm.[2,4]

The activity of HIF transcription factors, which consist of an O_2-regulated α-subunit (either HIF-1α, HIF-2α or HIF-3α) and a constitutively expressed β-subunit,[5] is controlled by PHD1, PHD2 and PHD3 dioxygenases, also known as egl nine homolog (EGLN) 2, EGLN1 and EGLN3 repectively.[6-9] Under normal O_2 conditions, the hydroxylation of specific proline residues within the continuously synthesized HIF-α subunit initiates its rapid proteasomal degradation via ubiquitylation by the von Hippel-Lindau (VHL)-E3 ubiquitin ligase complex, resulting in very low or non-detectable cellular HIF-α levels. Under hypoxia or following the administration of HIF-PHIs, the activity of HIF-PHDs and the rate of HIF-α degradation are reduced. This results in cellular HIF-α accumulation, the formation of HIF-α/β heterodimers in the nucleus and the increased transcription of O_2-regulated genes, such as *EPO*, vascular endothelial growth factor A (*VEGFA*), phosphoglycerate kinase 1 (*PGK1*), lactate dehydrogenase (*LDH*) and genes involved in the regulation of vascular tone such as nitric oxide synthase (*NOS*).[8,10]

The HIF system plays a major role in the regulation of vascular tone. In the pulmonary vasculature, hypoxia and HIF activation promote the development of pulmonary arterial hypertension through increased expression of vasoconstrictive factors, ion channels and ion transporters,[11] whereas hypoxia and HIF activation in other vascular beds are associated with vasodilation, e.g., in the muscle or skin, promoting blood flow.[12] Little is known about the effects of systemic pharmacological HIF activation on renal haemodynamics, O_2 metabolism and tubular transport efficiency. In this cross-sectional study, we investigated two HIF-PHIs, roxadustat (FG-4592) and molidustat (BAY 85-3934), which have been approved for the treatment of renal anaemia in Japan.[1] Our data provide novel insights into the effects of short-term systemic HIF activation on renal haemodynamics and O_2 metabolism and identify nitric oxide (NO) as a major mediator of these effects.

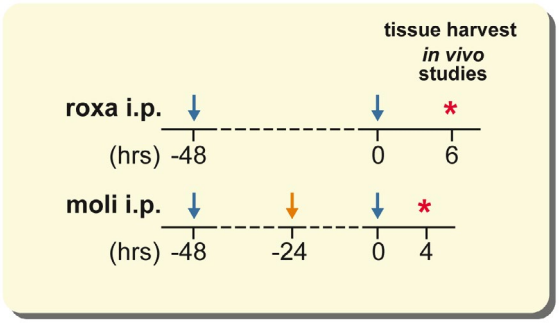

FIGURE 1 HIF-PHI administration schedule. Schematic illustrating the timing of drug administration (arrows) in relation to the time point of the in vivo analysis or tissue harvest (red asterisk). Blue arrows denote drug or vehicle administration for all cohorts, the orange arrow indicates that an additional dose was given for the molidustat 1 mg kg^{-1} cohort at the -24-h time point. i.p., intraperitoneal; moli, molidustat; roxa, roxadustat

2 | RESULTS

2.1 | Systemic pharmacological HIF activation increases RBF, GFR and tubular sodium transport

Roxadustat and molidustat are potent inhibitors of HIF-PHDs. They stabilize both, HIF-1α and HIF-2α and stimulate the production of endogenous EPO in patients with CKD.[1] To study the effects of short-term HIF-PHI administration on renal haemodynamics, different doses of roxadustat or molidustat were injected intraperitoneally (i.p.) into healthy male Sprague Dawley rats. Two injections were administered 48 hours apart, except for molidustat dosed at 1 mg kg^{-1}, which was given three times. The drug dosing schemes are outlined in Figure 1 and reflect published pharmacokinetic data in rats and humans.[13-15] In vivo experiments were performed 4 or 6 hours after the final HIF-PHI dose was administered (Figure 1).

We invasively measured blood pressure (BP) and heart rate (HR) in anaesthetized rats by femoral artery catheterization (Figure 2A). Treatment with both roxadustat or molidustat resulted in dose-dependent differences in systolic and diastolic BP without affecting HR. Mean arterial pressure (MAP) was 94 ± 2 mm Hg for roxadustat 30 mg kg^{-1} and 94 ± 2 mm Hg for molidustat 10 mg kg^{-1} vs 115 ± 2 mm Hg for vehicle control (Table 1 and Figure 2B).

We next investigated to what degree the HIF-PHI-induced reduction in MAP affected renal perfusion. We used Doppler ultrasonography to assess renal blood flow (RBF) and found significant dose-dependent differences in RBF for roxadustat dosed at 10 and 30 mg kg^{-1} and molidustat dosed at 10 mg kg^{-1},

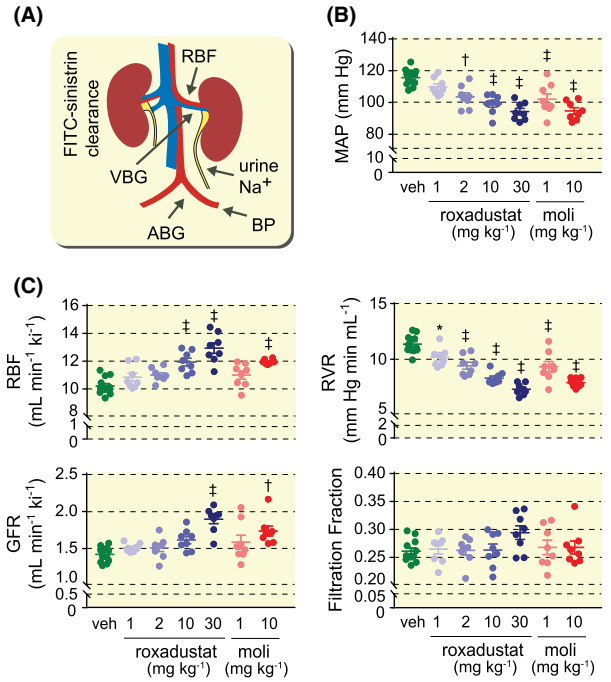

FIGURE 2 Systemic HIF-PHI administration increases renal blood flow and glomerular filtration. (A) Schematic illustrating the anatomic sites of haemodynamic measurements and blood or urine collections; aorta, arteries are shown in red, inferior vena cava and renal veins in blue, ureter and renal pelvis are shown in yellow. (B) Mean arterial pressure (MAP) readings from femoral artery in vehicle-treated control and HIF-PHI-treated cohorts. (C) Renal blood flow (RBF) per kidney, renal vascular resistance (RVR), glomerular filtration rate (GFR) assessed by means of FITC sinistrin clearance and filtration fraction in vehicle-treated and HIF-PHI-treated cohorts. Data are represented as mean ± SEM; one-way ANOVA followed by Tukey's post-hoc analysis; n = 12 for vehicle control, n = 8 for all other cohorts; $^{*}P < .05$, $^{\dagger}P < .01$ and $^{\ddagger}P < .001$ compared with vehicle control. ABG, arterial blood gas (femoral artery); BP, blood pressure (femoral artery); moli, molidustat; VBG, venous blood gas (left renal vein); veh, vehicle

indicating a change in renovascular resistance (RVR). RBF was 12.9 ± 0.4 mL min^{-1} per kidney for roxadustat dosed at 30 mg kg^{-1} and 11.9 ± 0.1 mL min^{-1} per kidney for molidustat dosed at 10 mg kg^{-1} vs 10.2 ± 0.2 mL min^{-1} per kidney for vehicle control. RVR decreased by 36% for roxadustat 30 mg kg^{-1} and by 30% for molidustat 10 mg kg^{-1} (Figure 2C).

Increased RBF was associated with a dose-dependent difference in glomerular filtration rate (GFR) as assessed by fluorescein isothiocyanate (FITC)-sinistrin clearance; GFR of 1.88 ± 0.06 mL min^{-1} per kidney for roxadustat 30 mg kg^{-1} and 1.73 ± 0.07 mL min^{-1} per kidney for molidustat 10 mg kg^{-1} vs 1.41 ± 0.03 mL min^{-1} per kidney for vehicle control (Figure 2C).

Because increased GFR enhances sodium delivery to the nephron, we examined tubular sodium transport rate (T_{Na}). To calculate T_{Na}, we determined the amount of filtered sodium and subtracted the amount of sodium that was excreted in the urine. T_{Na} was tightly correlated with GFR across all treatment groups (Figure 3) and was increased in the high-dose HIF-PHI cohorts compared to lower doses (Table 2). T_{Na} was increased by ~30% for roxadustat 30 mg kg^{-1} and by ~20% for molidustat 10 mg kg^{-1}; 263.4 ± 7.9 µmol min^{-1} per kidney and 240.3 ± 8.8 µmol min^{-1} per kidney, respectively, vs 196.2 ± 4.3 µmol min^{-1} per kidney for vehicle control. Increased T_{Na} in the high-dose roxadustat cohort was furthermore associated with increased urine flow (Table 2). No significant differences between cohorts were found with regard to filtration fraction (FF) and blood urea nitrogen (BUN) levels (Figure 2C and Table 1).

2.2 | High-dose HIF-PHI administration increases O_2 consumption disproportionally

Most of the O_2 consumed by the kidney is used for sodium transport and is in linear relationship to tubular sodium reabsorption.[16,17] Because HIF-PHI administration increased T_{Na}, we asked whether and to what degree HIF-PHI treatment affected renal O_2 consumption (QO_2) and tubular sodium transport efficiency (T_{Na}/O_2), the latter being a measure of metabolic efficiency, ie the amount of O_2 required to reabsorb a given amount sodium. We calculated O_2 content in arterial and renal vein blood arriving at O_2 delivery and QO_2 by multiplying with RBF. Not surprisingly, we found a dose-dependent increase in O_2 delivery; 2.5 ± 0.1 mL min^{-1} per kidney for roxadustat 30 mg kg^{-1} (~40% increase) and 2.1 ± 0.04 mL min^{-1} per kidney for molidustat 10 mg kg^{-1} (~18% increase) vs 1.8 ± 0.04 mL min^{-1} per kidney for vehicle control (Figure 3). Renal QO_2 was significantly increased for roxadustat 30 mg kg^{-1} and molidustat 10 mg kg^{-1} with 0.45 ± 0.06 mL min^{-1} for roxadustat 30 mg kg^{-1} and 0.34 ± 0.04 mL min^{-1} for molidustat 10 mg kg^{-1} vs 0.19 ± 0.01 mL min^{-1} for vehicle control but not for lower doses of roxadustat and molidustat (Figure 3). To assess metabolic efficiency, we calculated the T_{Na}/QO_2 ratio. Although we did not detect significant differences in T_{Na}/QO_2 for the roxadustat 1, 2 and 10 mg kg^{-1} and molidustat 1 mg kg^{-1} cohorts, T_{Na}/QO_2 was decreased by ~40% for the roxadustat 30 mg kg^{-1} and by ~30% for the molidustat 10 mg kg^{-1} cohort, suggesting that metabolic efficiency of tubular sodium transport was reduced for high-dose but not for low-dose HIF-PHI treatment (Figure 3).

2.3 | Systemic administration of HIF-activating compounds increases the expression of HIF-regulated genes in a dose-dependent manner

To assess the degree of HIF activation, we examined serum EPO levels and HIF target gene expression in kidney and liver

TABLE 1 Haemodynamic and blood parameters in vehicle- and HIF-PHI-treated cohorts

	Vehicle	R1	R2	R10	R30	M1	M10
N	12	8	8	8	8	8	8
HR (beats min^{-1})	336 ± 21	333 ± 17	371 ± 10	350 ± 21	337 ± 22	330 ± 10	381 ± 10
syst. BP (mm Hg)	144 ± 2	138 ± 2	131 ± 3†	128 ± 2‡	122 ± 2‡	130 ± 4‡	122 ± 2‡
diast. BP (mm Hg)	102 ± 1	95 ± 2	89 ± 2‡	85 ± 2‡	80 ± 2‡	87 ± 3‡	80 ± 2‡
BUN (mg dL^{-1})	36.5 ± 1.6	38.5 ± 1.4	37.6 ± 1	36.9 ± 2.2	37.6 ± 2.0	328 ± 1.4	39.6 ± 4.9
paO_2 (kPa)	8.6 ± 0.2	8.8 ± 0.2	8.6 ± 0.3	8.0 ± 0.1	8.5 ± 0.3	8.5 ± 0.2	8.2 ± 0.1
SaO_2 (%)	92 ± 1	93 ± 0	92 ± 0	91 ± 1	92 ± 1	92. ± 1	92 ± 1
Hb (g dL^{-1}) *arterial*	14.4 ± 0.2	14.5 ± 0.3	14.8 ± 0.3	14.6 ± 0.2	16.2 ± 0.4‡	13.8 ± 0.3	14.5 ± 0.2

Note: Data are represented as mean ± SEM; one-way ANOVA followed by Tukey's post-hoc analysis.

Abbreviations: BP, blood pressure; BUN, blood urea nitrogen; Hb, haemoglobin; HR, heart rate; paO_2, partial arterial O_2 pressure (femoral artery); SaO_2, percentage arterial haemoglobin saturation with O_2.

†$P < .01$.

‡$P < .001$ compared with vehicle control.

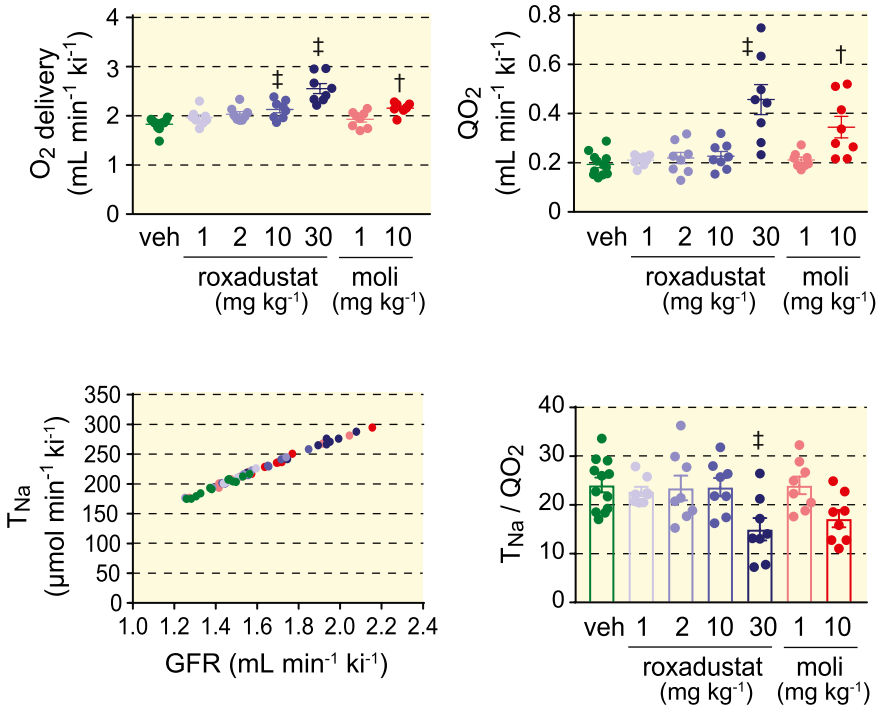

FIGURE 3 High-dose HIF-PHI treatment increases renal O_2 consumption disproportionally and reduces metabolic efficiency. Upper panels, O_2 delivery to the left kidney expressed as volume of O_2 (mL) delivered per minute per kidney (ki) and renal O_2 consumption rate (QO_2) expressed as volume of consumed O_2 (mL) per minute per kidney. Left lower panel, tubular sodium transport rate (T_{Na}) in relation to GFR per kidney; shown are the data for all animals in the study. Colour scheme used here corresponds to the colour schemes used in the other panels. Right lower panel, tubular transport efficiency assessed as transported sodium per consumed O_2 (T_{Na}/QO_2). For ratio calculations, QO_2 was converted from mL min^{-1} to µmol min^{-1}. Data are represented as mean ± SEM; one-way ANOVA followed by Tukey's post-hoc analysis; n = 12 for vehicle control, n = 8 for all other groups; †$P < .01$ and ‡$P < .001$ compared with vehicle control. moli, molidustat; veh, vehicle

from HIF-PHI-treated rats subjected to haemodynamic studies. We found dose-dependent differences in serum EPO levels compared to vehicle-treated rats, which was manifested in a ~6-fold increase in serum EPO for roxadustat dosed at 2 mg kg^{-1} and a ~130-fold increase for roxadustat dosed at 30 mg kg^{-1}. Approximately 5-fold and 70-fold greater serum EPO concentrations were measured in rats treated with molidustat dosed at 1 mg kg^{-1} and 10 mg kg^{-1}, respectively, compared with vehicle-treated controls. Differences in serum EPO levels were mirrored in kidney and liver *Epo* transcript levels (Figure 4A). Increased *Epo* expression was also found in other organs such as the lung and heart (Figure S1).

TABLE 2 Urine parameters per kidney in vehicle- and HIF-PHI-treated cohorts

	Vehicle	R1	R2	R10	R30	M1	M10
N	12	8	8	8	8	8	8
P_{Na} (mmol L^{-1})	139 ± 0.5	140 ± 0.5	140.6 ± 0.3	140 ± 0.4	140 ± 0.6	140 ± 0.6	139 ± 0.6
U_{Na} (mmol L^{-1})	59 ± 7	56 ± 7	61 ± 10	63 ± 8	60 ± 13	60 ± 6.0	58 ± 10
$U\dot{V}$ (µL min^{-1})	5.5 ± 0.6	6.3 ± 0.4	6.3 ± 0.8	7.5 ± 0.4	9.2 ± 0.8†	5.8 ± 0.7	7.4 ± 0.6
T_{Na} (µmol min^{-1})	196.2 ± 4.3	209.0 ± 3.0	211.0 ± 5.9	223.9 ± 7.0	263.4 ± 7.9‡	219.4 ± 12.9	240.3 ± 8.8‡
Na excretion (µmol min^{-1})	0.3 ± 0.1	0.4 ± 0.1	0.4 ± 0.1	0.5 ± 0.1	0.6 ± 0.1	0.4 ± 0.1	0.4 ± 0.1
FE_{Na} (%)	0.17 ± 0.04	0.17 ± 0.02	0.19 ± 0.04	0.21 ± 0.03	0.22 ± 0.05	0.16 ± 0.02	0.18 ± 0.03

Note: Data are represented as mean ± SEM; one-way ANOVA followed by Tukey's post-hoc analysis.

Abbreviations: FE_{Na}, fractional excretion of sodium (calculated per kidney); P_{Na}, serum sodium concentration; T_{Na}, tubular sodium transport per kidney; $U\dot{V}$, urine flow rate per kidney; U_{Na}, urine sodium concentration (left ureter).

†$P < .01$.

‡$P < .001$ compared with vehicle control.

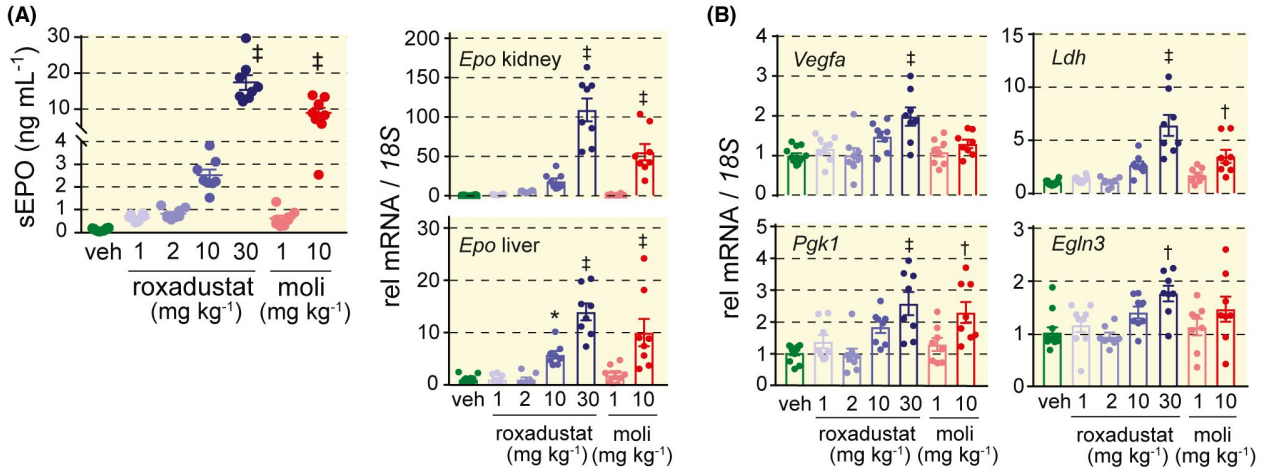

FIGURE 4 Dose-dependent HIF target gene activation following systemic HIF-PHI administration. (A) Serum erythropoietin (sEPO) and *Epo* mRNA levels in renal cortex and liver by qPCR in vehicle- and HIF-PHI-treated groups. (B) Transcript levels of vascular endothelial growth factor A (*Vegfa*), phosphoglycerate kinase 1 (*Pgk1*), lactate dehydrogenase (*Ldh*) and egl-9 family hypoxia-inducible factor 3 (*Egln3*) in total renal cortex homogenates. Data are represented as mean ± SEM; one-way ANOVA followed by Tukey's post-hoc analysis; n = 12 for vehicle control, n = 8 for all other groups; *$P < .05$, †$P < .01$ and ‡$P < .001$ compared with vehicle control. *18S*, 18S ribosomal RNA; i.p., intraperitoneal; moli, molidustat; roxa, roxadustat; veh, vehicle

Systemic administration of roxadustat resulted in stabilization of HIF-1α and HIF-2α in the kidney (Figure S2). In addition to renal *Epo*, which is regulated by HIF-2,[18] we detected significant increases in the expression of genes that are either predominantly HIF-1-depedent or co-regulated by HIF-1 and by HIF-2. These included adrenomedullin 1 (*Adm1*), BCL2 interacting protein 3 (*Bnip3*), *Egln3*, *Ldh*, pyruvate dehydrogenase kinase 1 (*Pdk1*), *Pgk1* and *Vegfa* (Figure 4B, Figures S3 and S4).[19] Systemic HIF activation was furthermore reflected in dose-dependent increases in the expression of HIF-regulated duodenal cytochrome B and divalent metal transporter 1 (Figure S5).

2.4 | High-dose HIF-PHI administration is associated with increased renal pO_2

In order to examine whether the decrease in T_{Na}/QO_2 in rats treated with high-dose roxadustat was associated with a reduction in tissue pO_2 levels, we measured cortical and medullary renal pO_2 in independent rat cohorts. Cortical tissue pO_2 was measured with a Clark-type electrode at 1 mm depth and medullary pO_2 at 4 mm depth below the renal capsule in vehicle-treated rats and in roxadustat-treated rats dosed at 10 or 30 mg kg^{-1}. Whereas cortical and medullary tissue pO_2 in the 10 mg kg^{-1} cohort was comparable to vehicle-treated

rats, cortical and medullary pO2 in the 30 mg kg^{-1} cohort were increased to 45.0 ± 0.5 mm Hg and 36.7 ± 0.5 mm Hg, respectively, vs 42.2 ± 0.6 mm Hg and 33.0 ± 0.4 mm Hg in control (Figure 5). Elevated renal pO_2 in the roxadustat 30 mg kg^{-1} cohort was associated with an increase in haemoglobin (Figure 5).

2.5 | Systemic HIF-PHI administration induces NOS expression and stimulates NO generation

NO plays a critical role in the regulation of renal haemodynamics and metabolic efficiency.[20,21] Since HIF-1 and HIF-2 have been shown to regulate nitric oxide synthesis,[22-24] we examined transcript levels of *Nos1*, *Nos2*, *Nos3*, arginase (*Arg*) 1 and *Arg2* in kidney, liver, heart, thoracic aorta, lung and primary lung endothelial cells (EC). We found that *Nos3* expression was significantly upregulated in kidneys from rats treated with high-dose roxadustat or molidustat. This was reflected in a comparable increase in renal NOS3 protein levels (Figure 6A). Although renal *Arg1* expression did not change in roxadustat and molidustat-treated cohorts, *Arg2* was upregulated by ~2-fold with molidustat 10 mg kg^{-1} but not with roxadustat (Figure 6A). To assess other tissues, we examined *Nos* and *Arg* transcript levels in lung, heart, liver and thoracic aorta. *Nos3* was significantly upregulated in total lung tissue, liver, thoracic aorta and primary lung EC isolated from rats treated with roxadustat 30 mg kg^{-1} (Figure 6B). In contrast, *Nos* expression in the heart did not change compared to control despite HIF activation as indicated by a significant increase in *Epo* transcript levels (Figure 6B and Figure S1).

To determine whether upregulation of *Nos* in the kidney and other tissues resulted in a detectable increase in NO generation, we measured nitrate and nitrite (NO metabolites) and creatinine in urine and calculated the NO/creatinine ratio. The urine NO/creatinine ratio was increased by 2.7- and 1.7-fold for roxadustat 30 mg kg^{-1} and molidustat 10 mg kg^{-1}, respectively, compared with vehicle control (Figure 7A).

2.6 | Inhibition of NO synthesis reverses HIF-PHI-induced haemodynamic changes

To examine the contribution of NO to HIF-PHI-induced changes in renal haemodynamic parameters, we administered NOS inhibitor Nω-nitro- L-arginine methyl ester (L-NAME) to rats pretreated with roxadustat dosed at 2 mg kg^{-1}, roxadustat dosed at 30 mg kg^{-1} or molidustat dosed at 10 mg kg^{-1}. L-NAME was administered i.p. following the final HIF-PHI injection. L-NAME treatment significantly decreased urine NO excretion in all HIF-PHI-treated cohorts, reaching low levels that were comparable to L-NAME-treated rats, which did not receive HIF-PHIs (Figure 7A). Because NO has been shown to inhibit the catalytic activity of HIF-PHDs,[8] we examined whether L-NAME had any effects on HIF-regulated gene expression. We found that the expression levels of representative HIF-regulated genes induced by HIF-PHI administration were not significantly different between L-NAME-treated rats and rats that did not receive L-NAME (Figure 7A), suggesting that L-NAME did not impact HIF-PHI-induced transcriptional responses in our model.

We next examined the effects of L-NAME on BP, RVR, RBF and GFR and urine parameters (Figure 7B and Figure S6). Although L-NAME reversed the haemodynamic effects induced by HIF-PHI administration in all treatment groups, reversal was only partial as differences in MAP, RVR, RBF and GFR were still detectable between the L-NAME-treated

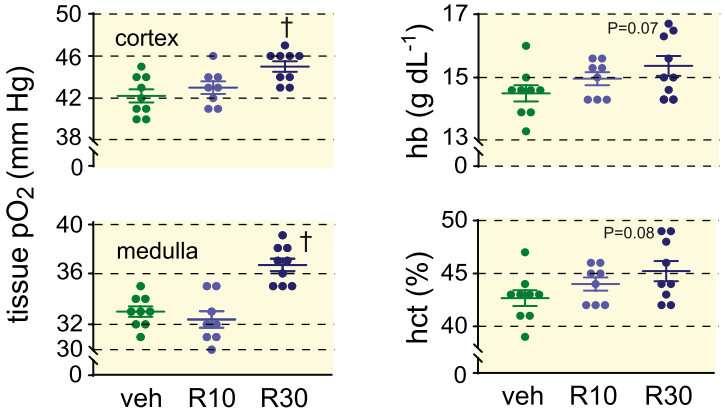

FIGURE 5 Systemic administration of high-dose HIF-PHI increases renal tissue pO_2. Left panels, tissue pO_2 measurements in renal cortex at 1mm depth and in renal medulla at 4 mm depth. Right panels, corresponding haemoglobin (hb) and hematocrit (hct) values. Hb and hct values for R30 are significantly different from vehicle control when analysed by Student's *t* test. Data are represented as mean ± SEM; one-way ANOVA followed by Tukey's post-hoc analysis; n = 8-9; $^{\dagger}P < .01$ compared with vehicle control. R10, roxadustat 10 mg kg^{-1}; R30 roxadustat 30 mg kg^{-1}; veh, vehicle

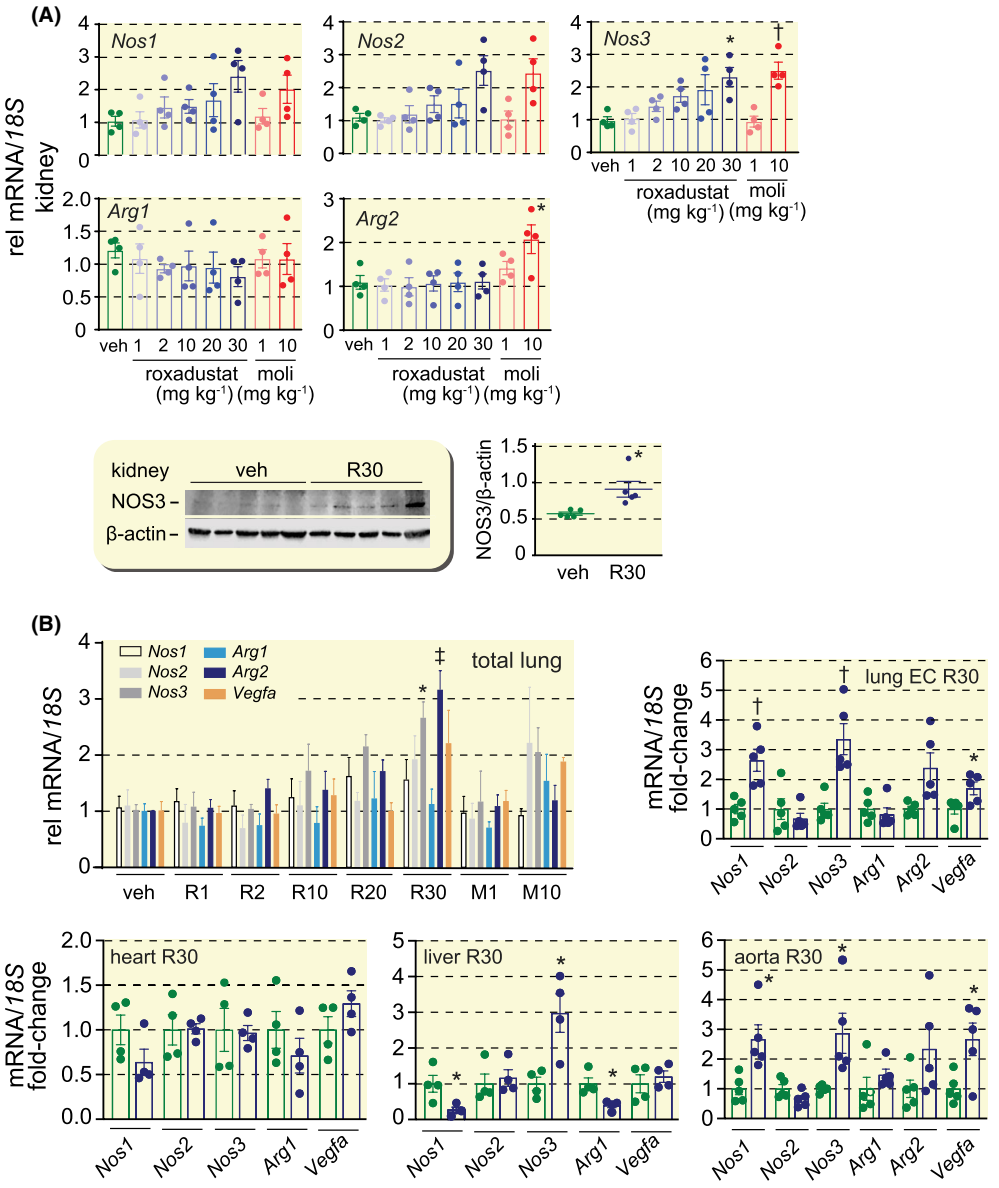

FIGURE 6 Systemic HIF-PHI administration induces nitric oxide synthase in multiple tissues. (A) Relative mRNA levels for nitric oxide synthase (*Nos*) 1, *Nos2*, *Nos3*, arginase (*Arg*)1 and *Arg2* as determined by qPCR in total kidney homogenates; n = 4 for all groups. Lower panel shows NOS3 and β-actin levels in whole renal cortex extracts by immunoblot for; n = 5 for vehicle- and roxadustat-treated groups. (B) Relative transcript levels of *Nos1*, *Nos2*, *Nos3*, *Arg1*, *Arg2* and vascular endothelial growth factor A (*Vegfa*) in total lung homogenates, primary lung endothelial cells (EC), heart, liver and thoracic aorta isolated from HIF-PHI-treated rats compared with vehicle-treated control; n = 4-5. *Arg2* transcripts were not detected in tissue homogenates from heart and liver. Data are represented as mean ± SEM; one-way ANOVA followed by Tukey's post-hoc analysis or Student's two-tailed *t* test used for NOS3/β-actin ratios and for mRNA expression panels lung EC R30, heart R30, liver R30 and aorta R30; $^{*}P < .05$, $^{\dagger}P < .01$ and $^{\ddagger}P < .001$ compared with vehicle control. M1, molidustat 1 mg kg^{-1}; M10, molidustat 10 mg kg^{-1}; moli, molidustat; R1, roxadustat 1 mg kg^{-1}; R2 roxadustat 2 mg kg^{-1}; R10, roxadustat 10 mg kg^{-1}; R20, roxadustat, 20mg kg^{-1}; R30, roxadustat 30 mg kg^{-1}; veh, vehicle

vehicle group and the L-NAME-treated HIF-PHI groups; GFR was 1.39 ± 0.07 mL min^{-1} per kidney for roxadustat dosed at 30 mg kg^{-1}, 1.29 ± 0.02 mL min^{-1} per kidney for molidustat 10 mg kg^{-1} and 1.14 ± 0.02 mL min^{-1} per kidney for vehicle-treated rats with $P < .001$ and < 0.05, respectively, by one-way ANOVA followed by Dunnett's multiple comparison test (Figure 7B).

3 | DISCUSSION

In this cross-sectional study, we investigated the effects of short-term pharmacological HIF activation on renal haemodynamics, O_2 metabolism and metabolic efficiency in healthy rats. We found that treatment with roxadustat or molidustat, two compounds which have completed phase 3 studies for

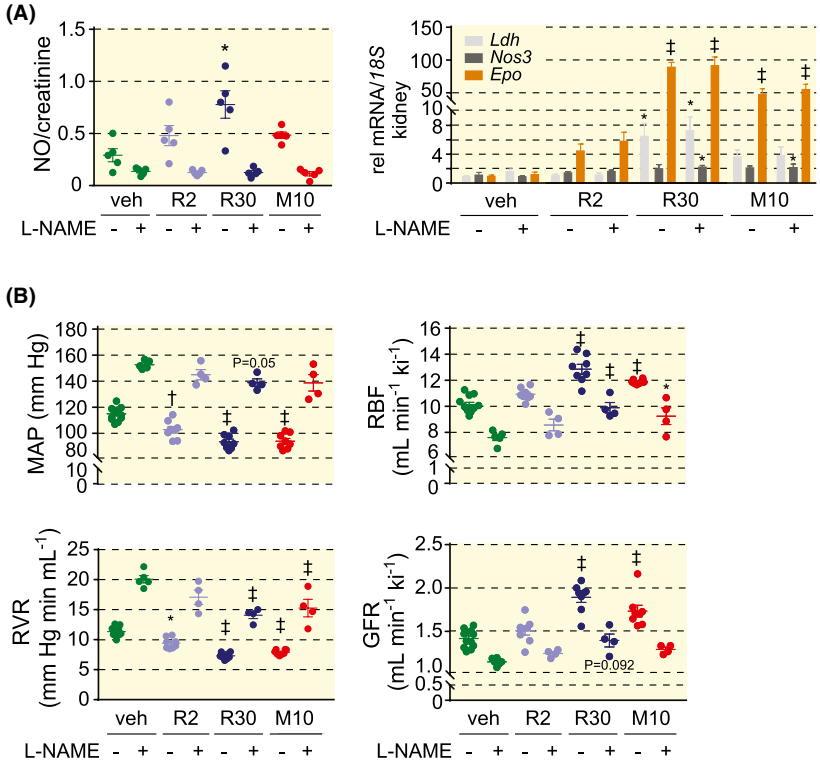

FIGURE 7 Pharmacological inhibition of NO synthesis suppresses HIF-PHI-induced hemodynamic changes. (A) Left panel, NO to creatinine ratio in urine from vehicle-treated control and HIF-PHI-treated rats in the absence (−) or presence (+) of L-NAME; n = 5. Right panel, HIF target gene expression in kidneys from HIF-PHI-treated rats compared with vehicle-treated rats in the absence (−) or presence (+) of L-NAME; n = 4. (B) Mean arterial pressure (MAP), renovascular resistance (RVR), renal blood flow (RBF) and glomerular filtration rate (GFR) for each treatment cohort in the absence (−) or presence (+) of L-NAME. L-NAME-treated cohorts were compared to the same experimental groups used in Figure 2; n = 12 for vehicle control, n = 4-5 for all cohorts treated with L-NAME, n = 8 for all other groups. Data are represented as mean ± SEM; two-way ANOVA followed by Tukey's post-hoc analysis; $^{*}P < .05$, $^{\dagger}P < .01$ and $^{\ddagger}P < .001$ compared to vehicle in the corresponding L-NAME group (− or +). *Epo*, erythropoietin; i.p., intraperitoneal; *Ldh*, lactate dehydrogenase; L-NAME, N_{ω}-Nitro-L-arginine methyl ester; M10, molidustat 10 mg kg^{-1}; *Nos3*, nitric oxide synthase 3; R2, roxadustat 2 mg kg^{-1}; R30, roxadustat 30 mg kg^{-1}; veh, vehicle

the treatment of renal anaemia, resulted in a dose-dependent increase in GFR, renal O_2 delivery and tubular sodium transport. These effects were partially mediated by the stimulation of NO synthesis. Larger HIF-PHI doses were associated with disproportionally higher rates of O_2 consumption, suggesting that pharmacological HIF activation beyond a certain level might be disadvantageous and attenuate metabolic efficiency in the kidney.

We demonstrate that short-term administration of HIF-PHIs roxadustat or molidustat lowered RVR and increased RBF and GFR in the absence of atmospheric hypoxia. Under hypobaric hypoxic conditions, changes in RBF, renal plasma flow (RPF) and GFR vary and depend on the acuteness of hypoxia exposure, the body's hydration state, the level of physical activity and whether polycythemia is present or not.[25-28] RPF is relatively more decreased than GFR in humans residing at high altitude, whereas both increases and reductions in GFR have been reported following acute ascent to high altitude.[25-28] Exposure of rats to chronic hypobaric hypoxia resulted in polycythemia and increased RBF and decreased RVR,[29,30] which correlated with the duration of hypoxia exposure and degree of polycythemia[30]; GFR remained relatively normal in these studies, despite the decrease in RPF. Of interest in this context are studies in a model of recombinant EPO-induced polycythemia, which raised the possibility that increased RBF under chronic hypoxia may be because of enhanced endothelial NO generation resulting from endothelial shear stress.[31] An increase in RBF was also found in rats exposed to acute hypoxia.[32] However, the kidney's ability to autoregulate regional blood flow at low perfusion pressures was reported to be diminished under these conditions and was associated with a decrease in medullary perfusion compared to normoxic conditions.[32] Whether and to what degree treatment with HIF-PHIs impacts on the autoregulation of regional blood flow in the kidney is unclear and warrants further investigation. In this regard, a better understanding of HIF-PHI actions on renal resistance vessels would be of importance, especially for patients with CKD who are at increased risk for developing acute kidney injury due to of hypotension.

In contrast with other organs, such as heart, muscle or brain, kidneys are relatively limited in their ability to match

metabolic demand by increasing O_2 delivery. A rise in RBF is associated with increased sodium filtration and tubular reabsorption and thus increased O_2 demand. The renal O_2 consumption rate QO_2 is an indirect measure of the kidney's metabolic activity, i.e., metabolic demand, and is in linear relationship with tubular sodium transport.[16] We found that QO_2 increased disproportionally compared with T_{Na} when high doses of roxadustat were administered (38% decrease in T_{Na}/QO_2), suggesting reduced metabolic efficiency. The reasons for this are not clear and may involve HIF-regulated shifts in tubular epithelial energy metabolism towards glycolysis.[33,34] HIF has also been shown to regulate mitochondrial function and the expression of electron transport chain (ETC) complexes, such as cytochrome c oxidase subunit 4 (COX4).[34,35] However, we did not find that short-term treatment with higher HIF-PHI doses affected the expression of COX4 or transcript levels of genes encoding ETC components (Figure S4).

A reduction in metabolic efficiency can lead to renal hypoxia.[36] Although, T_{Na}/QO_2 was decreased in rats treated with high-dose roxadustat, we found that renal tissue pO_2 was increased. This was most likely because of increased haemoglobin, i.e., O_2-carrying capacity, in roxadustat-treated rats. However, it is plausible that high-dose HIF-PHI treatment may cause or exacerbate renal hypoxia in the presence of anaemia and/or pathological conditions that decrease metabolic efficiency in the kidney, such as relative NO deficiency and oxidative stress,[20,36-39] abnormalities in mitochondrial metabolism,[40] and cellular and molecular alterations in transport processes shifting the sites of sodium reabsorption towards less energy-efficient distal nephron segments.[41]

Our data suggest that increased NO generation is a significant contributor to HIF-PHI-induced changes in renal haemodynamic parameters. HIF-1 and HIF-2 regulate the transcription of inducible NOS (*NOS2*) and endothelial NOS (*NOS3*) directly,[22-24] with NOS3 being particularly important for the regulation of renal haemodynamics and pathogenesis of kidney diseases.[42-46] We found that pharmacological NOS blockade with L-NAME reversed HIF-PHI-mediated haemodynamic effects substantially but not completely, suggesting that additional signalling pathways must have contributed to HIF-PHI-mediated changes in renal haemodynamics. This notion is supported by results from genome-wide mRNA expression analysis of kidneys from HIF-PHI-treated rats, which identified 322 differentially regulated genes involved the regulation of BP and vascular tone (Table S2). Adrenomedullin and VEGF are HIF-induced oxygen-sensitive vasodilatory proteins,[47,48] which have been shown to regulate renal haemodynamics.[49,50] *Vegfa* and *Adm1* transcript levels were increased in kidneys from HIF-PHI-treated rats and may have contributed HIF-PH-mediated haemodynamic effects directly or indirectly. Adrenomedullin increases RBF, enhances diuresis and promotes natriuresis[49,51] and VEGF has been shown to increase RBF.[50] Furthermore, adrenomedullin and VEGF stimulate the synthesis and release of NO in vascular smooth muscle and endothelial cells, respectively.[52-54]

In our studies, lower HIF-PHI doses were sufficient for the activation of renal *Epo* transcription, whereas the induction of other HIF-regulated genes appeared to require higher HIF-PHI doses. These findings are in line with the notion that the thresholds for HIF target gene induction are gene-dependent, with *EPO* being particularly sensitive to HIF activation under hypoxic conditions.[55] A 6- to 22-fold increase in serum EPO was reported for patients following the oral administration of 1 and 2 mg kg^{-1} of roxadustat, which is comparable to the 6 to 19-fold increase in serum EPO that we observed in rats treated with 2 and 10 mg kg^{-1} of roxadustat, respectively.[56] Our study results are therefore relevant to patients with CKD anaemia treated with HIF-PHIs. Preliminary data from pooled phase 3 studies in patients not on dialysis have suggested that roxadustat may increase GFR and delay time to initiation of renal replacement therapy.[1] Although preliminary, these data would be consistent with findings in our studies.

In conclusion, our studies provide novel insights into the effects of pharmacological HIF activation on renal haemodynamics and identify NO as a major mediator of these effects. Our findings provide strong rational for additional investigations into the role of systemic HIF activation in renal energy homeostasis and O_2 metabolism and for clinical studies that assess renal haemodynamics and NO metabolism in patients treated with HIF-PHIs.

4 | MATERIALS AND METHODS

4.1 | Animal handling and general procedure overview

Eight to 12-week-old male Sprague Dawley rats weighing 300-350 g were purchased from Charles River, Germany. Rats had free access to standard chow (Lantmannen, Kimstad, Sweden) and water. For surgical procedures, rats were anaesthetized with 120 mg kg^{-1} of thiobutabarbital (Inactin®; Sigma-Aldrich, Steinheim, Germany). All surgical procedures were performed on a temperature-controlled operating station to maintain body temperature at 37°C. Spontaneous breathing was facilitated by placement of a tracheostomy tube. Rats were euthanized by intravenous injection of saturated KCl solution and kidneys, liver, heart and lung were harvested for further analyses.

All animal handling and procedures were performed in accordance with European Guidelines for the Care and Use of Laboratory Animals and were reviewed, approved and monitored by the regional Animal Care and Ethics Committee responsible for Uppsala University (5.8.18-06724/2018).

4.2 | Drug administration

Roxadustat or molidustat were dissolved in vehicle [10% ethanol (70% grade) and 90% corn oil] and administered i.p.; roxadustat (FG-4592, Cayman Chemical, Ann Arbor, MI, USA) at a dose of 1, 2, 10, 20 or 30 mg kg^{-1}; molidustat (BAY 85-3934, Cayman Chemical, MI Ann Arbor, USA) at a dose of 1 or 10 mg kg^{-1}. Given its longer half-life, two doses of roxadustat were administered 48 hours apart, with the second dose given 6 hours prior to tissue harvest or initiation of surgical procedures. Three doses of 1 mg kg^{-1} of molidustat were administered 24 hours apart and two doses of 10 mg kg^{-1} of molidustat were given 48 hours apart, with the final doses given 4 hours prior to tissue harvest or initiation of surgical procedures. L-NAME (Sigma-Aldrich, Steinheim, Germany) was dissolved in the same vehicle and was injected i.p. at a dose of 10 mg kg^{-1} on the day of surgery at the time of final HIF-PHI administration.

4.3 | In vivo studies

Eight to 12 rats were randomly assigned to experimental cohorts and treated with either vehicle or HIF-PHI. GFR was assessed in anaesthetized rats prior to abdominal surgery by means of measuring FITC-sinistrin clearance utilizing the MediBeacon transdermal detection system, which was placed on the shaved chest (MediBeacon, Mannheim, Germany). Background measurements were obtained over a period of 5 minutes prior to tail vein injection of FITC-sinistrin (5 mg 100 g^{-1} body weight). Blood FITC-sinistrin concentrations were recorded transdermally over 30-45 minutes and FITC-sinistrin clearance was calculated according to the manufacturer's instructions using software provided by MediBeacon.

After completion of GFR measurements, a polyethylene catheter (AgnTho's, Stockholm, Sweden) was inserted into the left femoral artery for invasive BP and HR measurements (ADInstruments, Sydney, Australia) and for obtaining arterial blood samples. Standard Ringer's solution (5 mL kg^{-1} hr^{-1}) was infused into the left femoral vein. After catheterization of the urinary bladder for urine drainage, the left kidney was exposed by flank incision, immobilized in a plastic cup and covered with a saline-soaked cotton pad. The left ureter was catheterized for urine collections. A Transonic Doppler ultrasound probe (Transonic Systems, Ithaca, NY, USA) was placed on the renal artery to assess RBF. Rats were allowed to recover from abdominal surgery for 45 minutes before initiation of haemodynamic measurements. Prior to study completion the left renal vein was catheterized for blood collections. Tissue was harvested for gene expression analysis after the study was completed.

Arterial BP and RBF were measured over a period of 30 minutes. Urine was continuously collected over this time period, and urine volume was determined gravimetrically. Arterial and venous blood samples were obtained after the completion of haemodynamic measurements. Blood gases, haemoglobin concentrations and serum chemistries were analyzed utilizing the iSTAT system (Abbott Laboratories, Green Oaks, IL, USA). Hematocrit was determined by capillary centrifugation using a Fresco 21 centrifuge (ThermoFisher Scientific, Waltham, MA, USA). Urine electrolyte concentrations were determined by flame photometry (IL543, Instrumentation Lab, Milan, Italy). Serum iron levels, UIBC, TIBC, total cholesterol, triglycerides and glucose were measured in renal vein blood. Measurements were performed by the Clinical Pathology Laboratory of the University Animal Hospital, Uppsala, Sweden. Serum EPO levels were measured as described below in blood collected at the end of studies.

4.4 | Calculations of in vivo parameters

Arterial and renal venous O_2 content (O_2ct) was determined by means of the following standard equation: O_2ct (mL dL^{-1}) = [Hb × 1.34 × (O_2sat × 0.01)] (pO_2 × 0.023), where Hb is the haemoglobin concentration in g dL^{-1}, O_2sat is the percentage saturation of haemoglobin with O_2, pO_2 is partial pressure of O_2 in kPa, 1.34 represents the Hüfner coefficient in mL g^{-1} and 0.023 represents the O_2 solubility coefficient in mL kPa^{-1} dL^{-1}. Renal O_2 delivery was estimated from the arterial O_2ct multiplied by RBF (mL min^{-1}) and renal QO_2 was estimated from the arterio-venous O_2ct difference multiplied by RBF. T_{Na} expressed in µmol min^{-1} was assessed by calculating (P_{Na} × GFR) − (U_{Na} × $\dot{U}V$), where P_{Na} represents serum sodium concentration in mmol L^{-1}, GFR represents glomerular filtration rate in mL min^{-1}, U_{Na} represents urine sodium concentration in mmol L^{-1} and $\dot{U}V$ represents urine flow rate in µL min^{-1}. FE_{Na} was estimated as the ratio of sodium clearance to GFR, expressed as percentage, [(U_{Na} × $\dot{U}V$/P_{Na})/GFR] × 100. RVR (mm Hg min mL^{-1}) was calculated as MAP (mm Hg) divided by RBF (mL min^{-1}). FF was estimated as GFR/[RBF × (1 − hematocrit)], where haematocrit is expressed as a decimal notation.

4.5 | Measurement of renal pO_2

Kidney pO_2 was measured in a dedicated cohort of vehicle or HIF-PHI-treated male Sprague Dawley rats (n = 8-9) using a Clark-type O_2 microelectrode with a tip diameter of 10 µm (Unisense, Aarhus, Denmark) as previously decribed.[57] In brief, the electrodes were two-point calibrated at 37°C in water saturated with either $Na_2S_2O_5$ or air. Microelectrodes were inserted into the renal tissue with the aid of a micromanipulator. A linear correlation was obtained between O_2

tension and the electric current. O_2 tension measurements were carried out at 1 mm (cortex) and 4 mm (medulla) distance from the renal surface. This procedure was repeated more than or equal to five times in each left kidney. The averages for each respective depth from one animal were then considered as one experiment in the statistical analysis.

4.6 | Serum EPO, BUN, nitrate/nitrite measurements

Serum EPO levels were measured with a commercially available ELISA kit following the manufacturer's instructions (R&D Systems, Minneapolis, MN, USA). BUN was determined with the Urea Nitrogen (BUN) Colorimetric Detection Kit according to the manufacturer's instructions (ThermoFisher Scientific, Waltham, MA, USA). NO generation was assessed using the Nitrate/Nitrite Colorimetric Assay Kit (cat. # 780001, Cayman Chemical, Ann Arbor, MI, USA) according to the manufacturer's protocol. Creatinine was measured with the Creatinine Colorimetric/Fluorometric Assay Kit (cat # K625, BiovisionInc, Milpitas, CA, USA) according to the manufacturer's instructions.

4.7 | RNA, DNA, protein analysis

Total RNA was extracted from whole tissue homogenates or from primary cells and purified utilizing the RNeasy Plus kit according to the manufacturer's instructions (Qiagen, Germany). RNA concentrations were measured with a NanoDrop microvolume spectrophotometer (ThermoFisher Scientific, Waltham, MA, USA) and subjected to reverse transcription using iScript™ cDNA Synthesis Kit (Bio-Rad Laboratories, Stockholm, Sweden). qPCR was performed on a Bio-Rad CFX96 platform using iTaq™ Universal SYBR® Green Supermix. The comparative Ct-method was used for the analysis of relative mRNA expression levels according to the manufacturer's instructions (Bio-Rad Laboratories, Stockholm, Sweden). Relative mRNA levels were expressed as a fold-change over control. *18S* ribosomal RNA was used as internal control. Primer sequences are listed in Table S1.

RNA sequencing analysis was performed with whole renal cortex extract obtained from a dedicated cohort of rats treated with roxadustat 2 mg kg^{-1} or 30 mg kg^{-1}, molidustat 10 mg kg^{-1} or vehicle on an Illumina 2000 NGS platform (Illumina, San Diego, CA, USA).

Protein samples were separated in a 4%-12% gradient SDS polyacrylamide gel (Bio-Rad Laboratories, Sweden, Stockholm), transferred to a polyvinylidene difluoride membrane (Merck Millipore, Burlington, VT, USA) and incubated sequentially with primary and secondary antibodies. Membranes were imaged using the Odyssey® Fc digital imaging system (LI-COR® Biosciences, Lincoln, NE, USA) and analysed with NIH ImageJ software (version 1.46). NOS3 was detected with anti-eNOS antibody [M221] (cat. # ab76198, Abcam, Cambridge, UK) at a dilution of 1:1000 and anti-mouse-IRDye 800CW (LI-COR® Biosciences, Lincoln, NE, USA) was used as secondary antibody at a dilution of 1:10 000. β-actin was detected with anti-β-actin antibody (C4) (cat. # sc-47778, Santa Cruz, Dallas, TX, USA). COX4 protein levels were assessed with anti-COX4 polyclonal rabbit antibody (cat. # NB110-39115, Novus Biologicals, Centennial, CO, USA) and with anti-COX IV Isoform 2 polyclonal goat antibody (cat. # NBP1-44068, Novus Biologicals, Centennial, CO, USA). α-tubulin was detected with anti-α-tubulin (DM1A) mouse monoclonal antibody (cat# 3873, Abcam, Cambridge, UK). Anti-rabbit IgG, peroxidase-linked species-specific whole antibody (cat. # 10794347, ThermoFisher Scientific, Waltham, MA, USA), anti-goat IgG (H + L) secondary HRP-conjugated polyclonal antibody (cat. # 31402, Invitrogen ThermoFisher Scientific, Waltham, MA, USA) and anti-mouse IgG peroxidase-linked polyclonal antibody (cat. # 10196124, ThermoFisher Scientific, Waltham, MA, USA) were used as secondary antibodies.

For HIF immunohistochemistry, formalin-fixed, paraffin-embedded kidney sections from rats and mice were stained with anti-HIF-1α polyclonal antibody (cat. # 10006421, Cayman Chemical Co., Ann Arbor, MI, USA) or anti-HIF2-α PM8 antiserum, a gift from Peter Ratcliffe (University of Oxford, Oxford, UK) as described previously.[58] For RNA fluorescent in situ hybridization, *Epo* transcripts were detected in formalin-fixed, paraffin-embedded kidney sections using Rn-Epo (cat. # 455901, Advanced Cell Diagnostics, Hayward, CA, USA) and the RNAscope® multiplex fluorescent kit according to the manufacturer's instructions.

4.8 | Isolation of rat lung endothelial cells

Rat lung endothelial cells were isolated from a dedicated cohort of rats as described previously.[59] In brief, animals were perfused with DMEM (cat. # 31053-028, Gibco-ThermoFisher Scientific, Waltham, MA, USA) and lungs were inflated with DMEM containing collagenase A at a final concentration of 2 mg mL^{-1} (cat. # 10103586001, Roche, Basel, Switzerland). Lung tissue was digested at 37°C with collagenase A (cat. # 10103586001, Roche, Basel, Switzerland) and DNAse (cat. # 18047-019, Invitrogen-ThermoFisher Scientific, Waltham, MA, USA); final concentrations of 2.5 mg μL^{-1} and 120 U mL^{-1}, respectively. Digested tissue material was then passed through a 40 μm cell strainer (cat. # 352340, BD Biosciences, San Jose, CA, USA) and centrifuged. Isolated cells were mixed with 30 μL of anti-CD31 precoated Dynabeads® (cat. # 11155D, ThermoFisher Scientific, Waltham, MA, USA)

and incubated on an orbital shaker for 20 minutes at 4°C. After washing, cells were lysed in RLT buffer (cat. # 74104, Qiagen, Hilden, Germany) and processed for RNA isolation and qPCR analysis.

4.9 | Statistical analysis

Statistical analysis was performed by either Student's two-tailed *t* test for two-group comparisons and by one or two-way ANOVA followed by Tukey's post-hoc analysis for multi-group comparisons; in addition, one-way ANOVA followed by Dunnett's multiple comparison test was performed (Prism 9, GraphPad Software, La Jolla, CA, USA); a *P* value of <.05 was considered statistically significant. All data are presented as mean ± SEM.

ACKNOWLEDGEMENTS

The data that support the findings of this study are available from the corresponding author upon reasonable request. RNAseq primary data sets are shared via geo@ncbi.nlm.nih.gov. The GSE identification number is: GSE 158908 This study was supported by funds from the Swedish Research Council, VINNOVA and Uppsala University. VHH holds the Krick-Brooks chair in Nephrology at Vanderbilt University. Open access funding enabled and organized by ProjektDEAL. The GSE identification number is: GSE158908.

CONFLICT OF INTEREST

The authors declare that no conflict of interest exists.

AUTHOR CONTRIBUTIONS

VHH conceived and designed the research studies. MB and VHH analyzed and interpreted the data, wrote the manuscript and made the figures. AF, AD, MB and HK performed experiments and acquired data. FP and AAU helped with the interpretation and analysis of data.

ORCID

Mikhail Burmakin https://orcid.org/0000-0002-1370-6251
Hanako Kobayashi https://orcid.org/0000-0001-5064-2616
Andrés A. Urrutia https://orcid.org/0000-0001-7945-5515
Fredrik Palm https://orcid.org/0000-0002-0127-3348
Volker H. Haase https://orcid.org/0000-0002-7051-8994

REFERENCES

1. Haase VH. Hypoxia-inducible factor-prolyl hydroxylase inhibitors in the treatment of anemia of chronic kidney disease. *Kidney Int Suppl*. 2021;11(1):8-25.
2. Schodel J, Ratcliffe PJ. Mechanisms of hypoxia signalling: new implications for nephrology. *Nat Rev Nephrol*. 2019;15(10):641-659.
3. Semenza GL. Oxygen sensing, homeostasis, and disease. *N Engl J Med*. 2011;365(6):537-547.
4. Sanghani NS, Haase VH. Hypoxia-inducible factor activators in renal anemia: current clinical experience. *Adv Chronic Kidney Dis*. 2019;26(4):253-266.
5. McIntosh BE, Hogenesch JB, Bradfield CA. Mammalian Per-Arnt-Sim proteins in environmental adaptation. *Annu Rev Physiol*. 2010;72:625-645.
6. Berra E, Benizri E, Ginouves A, Volmat V, Roux D, Pouyssegur J. HIF prolyl-hydroxylase 2 is the key oxygen sensor setting low steady-state levels of HIF-1alpha in normoxia. *Embo J*. 2003;22(16):4082-4090.
7. Appelhoff RJ, Tian YM, Raval RR, et al. Differential function of the prolyl hydroxylases PHD1, PHD2, and PHD3 in the regulation of hypoxia-inducible factor. *J Biol Chem*. 2004;279(37):38458-38465.
8. Kaelin WG, Ratcliffe PJ. Oxygen sensing by metazoans: the central role of the HIF hydroxylase pathway. *Mol Cell*. 2008;30(4):393-402.
9. Ivan M, Kaelin WG. The EGLN-HIF O. *Mol Cell*. 2017;66(6):772-779.
10. Semenza GL. Hypoxia-inducible factors in physiology and medicine. *Cell*. 2012;148(3):399-408.
11. Shimoda LA, Yun X, Sikka G. Revisiting the role of hypoxia-inducible factors in pulmonary hypertension. *Curr Opin Physiol*. 2019;7:33-40.
12. Cowburn AS, Takeda N, Boutin AT, et al. HIF isoforms in the skin differentially regulate systemic arterial pressure. *Proc Natl Acad Sci USA*. 2013;110(43):17570-17575.
13. Flamme I, Oehme F, Ellinghaus P, Jeske M, Keldenich J, Thuss U. Mimicking hypoxia to treat anemia: HIF-Stabilizer BAY 85–3934 (Molidustat) stimulates erythropoietin production without hypertensive effects. *PLoS One*. 2014;9(11):e111838.
14. Groenendaal-van de Meent D, Adel M, Noukens J, et al. Effect of moderate hepatic impairment on the pharmacokinetics and pharmacodynamics of roxadustat, an oral hypoxia-inducible factor prolyl hydroxylase inhibitor. *Clin Drug Invest*. 2016;36(9):743-751.
15. Bottcher M, Lentini S, Arens ER, et al. First-in-man-proof of concept study with molidustat: a novel selective oral HIF-prolyl hydroxylase inhibitor for the treatment of renal anaemia. *Br J Clin Pharmacol*. 2018;84(7):1557-1565.
16. Deetjen P, Kramer K. The relation of O2 consumption by the kidney to Na re-resorption. *Pflugers Arch Gesamte Physiol Menschen Tiere*. 1961;273:636-650.
17. Mandel LJ, Balaban RS. Stoichiometry and coupling of active transport to oxidative metabolism in epithelial tissues. *Am J Physiol*. 1981;240(5):F357-371.
18. Kobayashi H, Liu Q, Binns TC, et al. Distinct subpopulations of FOXD1 stroma-derived cells regulate renal erythropoietin. *J Clin Invest*. 2016;126(5):1926-1938.
19. Keith B, Johnson RS, Simon MC. HIF1alpha and HIF2alpha: sibling rivalry in hypoxic tumour growth and progression. *Nat Rev Cancer*. 2012;12(1):9-22.
20. Welch WJ, Baumgartl H, Lubbers D, Wilcox CS. Renal oxygenation defects in the spontaneously hypertensive rat: role of AT1 receptors. *Kidney Int*. 2003;63(1):202-208.
21. Deng A, Miracle CM, Suarez JM, et al. Oxygen consumption in the kidney: effects of nitric oxide synthase isoforms and angiotensin II. *Kidney Int*. 2005;68(2):723-730.
22. Melillo G, Musso T, Sica A, Taylor LS, Cox GW, Varesio L. A hypoxia-responsive element mediates a novel pathway of

activation of the inducible nitric oxide synthase promoter. *J Exp Med*. 1995;182(6):1683-1693.
23. Coulet F, Nadaud S, Agrapart M, Soubrier F. Identification of hypoxia-response element in the human endothelial nitric-oxide synthase gene promoter. *J Biol Chem*. 2003;278(47):46230-46240.
24. Rodriguez-Miguelez P, Lima-Cabello E, Martinez-Florez S, Almar M, Cuevas MJ, Gonzalez-Gallego J. Hypoxia-inducible factor-1 modulates the expression of vascular endothelial growth factor and endothelial nitric oxide synthase induced by eccentric exercise. *J Appl Physiol*. 2015;118(8):1075-1083.
25. Lozano R, Monge C. Renal function in high-altitude natives and in natives with chronic mountain sickness. *J Appl Physiol*. 1965;20(5):1026-1027.
26. Olsen NV, Kanstrup IL, Richalet JP, Hansen JM, Plazen G, Galen FX. Effects of acute hypoxia on renal and endocrine function at rest and during graded exercise in hydrated subjects. *J Appl Physiol*. 1992;73(5):2036-2043.
27. Luks AM, Johnson RJ, Swenson ER. Chronic kidney disease at high altitude. *J Am Soc Nephrol*. 2008;19(12):2262-2271.
28. Pichler J, Risch L, Hefti U, et al. Glomerular filtration rate estimates decrease during high altitude expedition but increase with Lake Louise acute mountain sickness scores. *Acta Physiol (Oxf)*. 2008;192(3):443-450.
29. Ou LC, Silverstein J, Edwards BR. Renal function in rats chronically exposed to high altitude. *Am J Physiol*. 1984;247(1 Pt 2):F45-F49.
30. Thron CD, Chen J, Leiter JC, Ou LC. Renovascular adaptive changes in chronic hypoxic polycythemia. *Kidney Int*. 1998;54(6):2014-2020.
31. Wilcox CS, Deng X, Doll AH, Snellen H, Welch WJ. Nitric oxide mediates renal vasodilation during erythropoietin-induced polycythemia. *Kidney Int*. 1993;44(2):430-435.
32. Flemming B, Seeliger E, Wronski T, Steer K, Arenz N, Persson PB. Oxygen and renal hemodynamics in the conscious rat. *J Am Soc Nephrol*. 2000;11(1):18-24.
33. Semenza GL. Regulation of metabolism by hypoxia-inducible factor 1. *Cold Spring Harb Symp Quant Biol*. 2011;76:347-353.
34. Farsijani NM, Liu Q, Kobayashi H, et al. Renal epithelium regulates erythropoiesis via HIF-dependent suppression of erythropoietin. *J Clin Invest*. 2016;126(4):1425-1437.
35. Fukuda R, Zhang H, Kim JW, Shimoda L, Dang CV, Semenza GL. HIF-1 regulates cytochrome oxidase subunits to optimize efficiency of respiration in hypoxic cells. *Cell*. 2007;129(1):111-122.
36. Palm F, Nordquist L. Renal tubulointerstitial hypoxia: cause and consequence of kidney dysfunction. *Clin Exp Pharmacol Physiol*. 2011;38(7):474-480.
37. Brezis M, Heyman SN, Dinour D, Epstein FH, Rosen S. Role of nitric oxide in renal medullary oxygenation. Studies in isolated and intact rat kidneys. *J Clin Invest*. 1991;88(2):390-395.
38. Welch WJ, Blau J, Xie H, Chabrashvili T, Wilcox CS. Angiotensin-induced defects in renal oxygenation: role of oxidative stress. *Am J Physiol Heart Circ Physiol*. 2005;288(1):H22-H28.
39. Deng A, Tang T, Singh P, et al. Regulation of oxygen utilization by angiotensin II in chronic kidney disease. *Kidney Int*. 2009;75(2):197-204.
40. Nordquist L, Friederich-Persson M, Fasching A, et al. Activation of hypoxia-inducible factors prevents diabetic nephropathy. *J Am Soc Nephrol*. 2015;26(2):328-338.
41. Hansell P, Welch WJ, Blantz RC, Palm F. Determinants of kidney oxygen consumption and their relationship to tissue oxygen tension in diabetes and hypertension. *Clin Exp Pharmacol Physiol*. 2013;40(2):123-137.
42. Mount PF, Power DA. Nitric oxide in the kidney: functions and regulation of synthesis. *Acta Physiol (Oxf)*. 2006;187(4):433-446.
43. Nakagawa T, Sato W, Glushakova O, et al. Diabetic endothelial nitric oxide synthase knockout mice develop advanced diabetic nephropathy. *J Am Soc Nephrol*. 2007;18(2):539-550.
44. Nakayama T, Sato W, Kosugi T, et al. Endothelial injury due to eNOS deficiency accelerates the progression of chronic renal disease in the mouse. *Am J Physiol Renal Physiol*. 2009;296(2):F317-F327.
45. Yuen DA, Stead BE, Zhang Y, et al. eNOS deficiency predisposes podocytes to injury in diabetes. *J Am Soc Nephrol*. 2012;23(11):1810-1823.
46. Baylis C. Arginine, arginine analogs and nitric oxide production in chronic kidney disease. *Nat Clin Pract Nephrol*. 2006;2(4):209-220.
47. Forsythe JA, Jiang BH, Iyer NV, et al. Activation of vascular endothelial growth factor gene transcription by hypoxia-inducible factor 1. *Mol Cell Biol*. 1996;16(9):4604-4613.
48. Garayoa M, Martinez A, Lee S, et al. Hypoxia-inducible factor-1 (HIF-1) up-regulates adrenomedullin expression in human tumor cell lines during oxygen deprivation: a possible promotion mechanism of carcinogenesis. *Mol Endocrinol*. 2000;14(6):848-862.
49. Ebara T, Miura K, Okumura M, et al. Effect of adrenomedullin on renal hemodynamics and functions in dogs. *Eur J Pharmacol*. 1994;263(1-2):69-73.
50. Klanke B, Simon M, Rockl W, Weich HA, Stolte H, Grone HJ. Effects of vascular endothelial growth factor (VEGF)/vascular permeability factor (VPF) on haemodynamics and permselectivity of the isolated perfused rat kidney. *Nephrol Dial Transplant*. 1998;13(4):875-885.
51. Rademaker MT, Charles CJ, Lewis LK, et al. Beneficial hemodynamic and renal effects of adrenomedullin in an ovine model of heart failure. *Circulation*. 1997;96(6):1983-1990.
52. Ikeda U, Kanbe T, Shimada K. Adrenomedullin increases inducible nitric oxide synthase in rat vascular smooth muscle cells stimulated with interleukin-1. *Hypertension*. 1996;27(6):1240-1244.
53. Shen BQ, Lee DY, Zioncheck TF. Vascular endothelial growth factor governs endothelial nitric-oxide synthase expression via a KDR/Flk-1 receptor and a protein kinase C signaling pathway. *J Biol Chem*. 1999;274(46):33057-33063.
54. van der Zee R, Murohara T, Luo Z, et al. Vascular endothelial growth factor/vascular permeability factor augments nitric oxide release from quiescent rabbit and human vascular endothelium. *Circulation*. 1997;95(4):1030-1037.
55. Sandner P, Gess B, Wolf K, Kurtz A. Divergent regulation of vascular endothelial growth factor and of erythropoietin gene expression in vivo. *Pflugers Arch*. 1996;431(6):905-912.
56. Besarab A, Provenzano R, Hertel J, et al. Randomized placebo-controlled dose-ranging and pharmacodynamics study of roxadustat (FG-4592) to treat anemia in nondialysis-dependent chronic kidney disease (NDD-CKD) patients. *Nephrol Dial Transplant*. 2015;30(10):1665-1673.
57. Palm F, Cederberg J, Hansell P, Liss P, Carlsson PO. Reactive oxygen species cause diabetes-induced decrease in renal oxygen tension. *Diabetologia*. 2003;46(8):1153-1160.
58. Kobayashi H, Liu J, Urrutia AA, et al. Hypoxia-inducible factor prolyl-4-hydroxylation in FOXD1 lineage cells is essential for normal kidney development. *Kidney Int*. 2017;92(6):1370-1383.

59. Jin Y, Muhl L, Burmakin M, et al. Endoglin prevents vascular malformation by regulating flow-induced cell migration and specification through VEGFR2 signalling. *Nat Cell Biol*. 2017;19(6):639-652.

SUPPORTING INFORMATION

Additional Supporting Information may be found online in the Supporting Information section.

How to cite this article: Burmakin M, Fasching A, Kobayashi H, et al. Pharmacological HIF-PHD inhibition reduces renovascular resistance and increases glomerular filtration by stimulating nitric oxide generation. *Acta Physiol*. 2021;00:e13668. https://doi.org/10.1111/apha.13668